# Reduced-order Robust Control of a Fuel Cell Air Supply System

David Hernández-Torres, Delphine Riu, Olivier Sename

# Reduced-order Robust Control of a Fuel Cell Air Supply System ⋆

**David Hernández-Torres** * **Delphine Riu** ** **Olivier Sename** ***

* *Université de Toulouse (INP, UPS; LAPLACE; CNRS); ENSEEIHT, 2 rue Charles Camichel, F-31071 Toulouse, France (e-mail: david.hernandez@laplace.univ-tlse.fr).*
** *G2ELab (UMR 5269 INPG-UJF-CNRS), 21 avenue des martyrs, 38031 Grenoble, France (e-mail: delphine.riu@g2elab.grenoble-inp.fr).*
*** *GIPSA-lab, INPG, Université Grenoble Alpes, 11 rue des mathématiques, 38402 Grenoble, France (e-mail: olivier.sename@gipsa-lab.grenoble-inp.fr).*

**Abstract:** This paper presents the design of several reduced order robust control strategies for the air supply of a hybrid fuel cell power generator. The management of the air dynamic entering the fuel cell is assured by the control of the air flow of a compressor. The air supply sub-system is controlled to keep a desired oxygen excess ratio, this allow to improve the fuel cell dynamic performance. Robustness analysis studies are performed, these robust properties are contrasted with classic control strategies, demonstrating the advantage of the multivariable reduced order robust methodologies.

*Keywords:* Robust control, multivariable control, fuel cells, hybrid power generators, air compressor.

## 1. INTRODUCTION

Fuel cells (FC) are electro-chemical devices that convert chemical energy into electrical energy by means of an electrode pair, an electrolyte and a catalyzer.

A fuel cell may not operate alone. When referring to a FC *system*, all the auxiliary systems, needed for operation, are included. This makes the complete system a rather complex structure to control. The auxiliary elements can be divided into two groups: electrical and thermo-dynamical management sub-systems. The first ensures the safe connection of the FC to the electrical application (load) and the second sub-system ensures the gas, water, air and thermal management of the FC. A complete robust control solution was presented by the authors in Hernandez-Torres et al. (2011). Of course, these sub-systems are both highly dependent, as the gas flow in the stack directly depends on the load current demand, then the electrical sub-system is influenced by the flow dynamics. In terms of the FC efficiency, the stack will have a better performance at higher flow pressures, but this means higher compression ratios and higher energy consumption of the compressor-motor sub-system, an a degraded overall system efficiency. An efficient control is necessary to guarantee an optimal management of hydrogen and air in the system, avoiding stack membrane degradation (and output voltage degradation) for a more reliable and efficient operation.

Within the context, a need is identified for a robust multivariable reduced order control approach to manage the thermo-dynamical sub-systems on the FC. The disturbance rejection approach is extensively adopted in this thesis, since, as a general proposition, this will have an influence on the cells life-span, avoiding non-desired high energy transients. It should be noted that limitations on the FC performance are due not only to material characteristics, but also on the optimization of the thermo-dynamical operating variables as, for example, the flow rate of reactant streams (Gasser, 2006). As a central part of the FC dynamic behaviour, the control of the compressor-motor and the supply air flow are considered. Several articles can be found in the literature addressing these problems. An interesting study on the air compressor control influence on the FC efficiency is presented in Tekin et al. (2006). Linear control of the thermo-dynamical system on a FC is studied using model-based control in Grujicic et al. (2004). Multivariable robust $\mathcal{H}_\infty$ and low order PID's controls are proposed in Wang et al. (2008) and Wang and Ko (2010) respectively. An LPV control approach for the FC air supply was presented in Hernandez-Torres et al. (2012). Non-linear control has also been used with good results using feed-back linearization and passivity in Na and Gou (2008) and Talj et al. (2009) respectively. Model predictive optimal control has also been used for this type of systems in Chang and Moura (2009).

In this work some assumptions are made to obtain simplified control-oriented models. The fuel flow control, the air humidification and the stack temperature controls are assumed to be perfect. Robust control is of special interest, aiming to achieve robust stability and performance for systems subject to uncertainties. In this paper we demonstrate the advantage of a multivariable reducer or-

⋆ This work was possible thanks to the financial support of the Grenoble Institute of Technology. Dr. Hernández-Torres formerly with G2ELab in Grenoble, is now with the University of Toulouse.

der control approach over the classical decoupled control methodologies and the validation with complete closed-loop robustness analysis.

## 2. SYSTEM MODEL AND PARAMETER IDENTIFICATION

### *2.1 Test bench setup for system model identification*

A test-bench fuel cell setup located in the Grenoble campus in France is used for model identification of the fuel cell air supply system. The test-bench is composed by different elements that allow to efficiently control, operate and visualize several parameters of the FCS such as: fluid dynamics (pressure, gas flow rates, reactant stoichiometric values, etc.), thermo-dynamic parameters (stack temperature, humidification rates, etc.), or even electrical parameters (single cell voltage, stack current and power). The test-bench used for identification with the real fuel cell stack is presented in Figure 1.

Fig. 1. Experimental setup used for identification.

The stack considered in this work is a PEMFC from French company Paxitech© and mounted on a UBzM© frame with a nominal power of 475W. The arrangement is composed by a 16-cell/100 $cm^2$ effective area stack. The air channel entering at the FC stack input is controlled by air flow and pressure regulators. For air flow control the setup is equipped with *Smart* series *5800S* models from *Brooks Instruments*©, with reading/regulation capabilities using $0-5$V control signals. For pressure reading purposes the test-bench is provided by series 21 *Keller*© piezoresistive transmitters. For the pressure reading/regulation option, a *VP50* proportional control valve from *Norgren*© was installed for air back-pressure control.

According to the requirements of the FCS in the test-bench, an air compressor was chosen to guarantee at least an air flow of 60 slpm [1] and a pressure range of $1-2$ bars (absolute). With these characteristics and allowing an over-sizing factor for future stack expansion in the test-bench, the Vairex© *VV-0520.08 INT* model dry fixed vane air compressor was chosen. The compressor has an operating range of $24-40$V and nominal power of $900-1200$W. The air flow ranges from $0.2-10$g/s at compression pressures of $1.1-2$ bars (abs). The compressor layout and the compressor map as given by manufacturer are given in Figures 2 and 3.

[1] Standard litres per minute

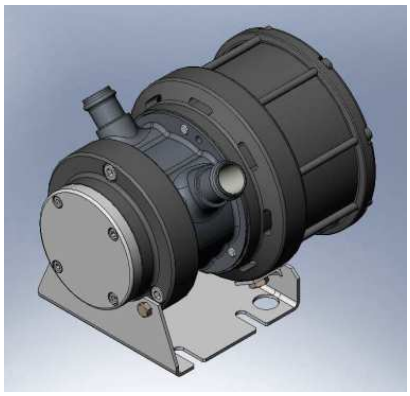

Fig. 2. Compressor layout.

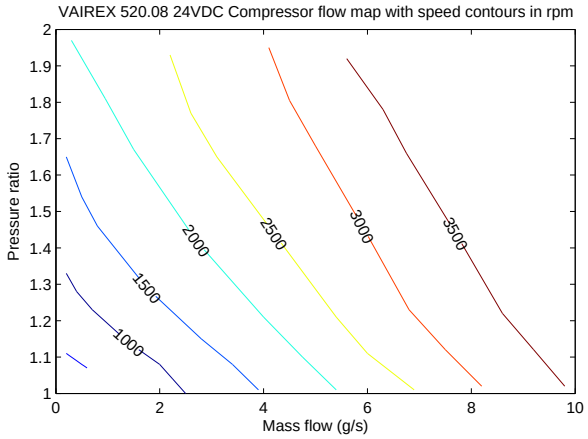


Fig. 3. Compressor operation map.

### *2.2 Air supply model*

Compressor modeling is somehow considered as the core of the fuel cell model. Two proposed models are presented in the following sections. First, the non-linear model proposed by Pukrushpan et al. (2004), and secondly, a linear model is proposed by Gasser (2006).

The first compressor model presented here is a non-linear compressor model proposed by Pukrushpan et al. (2004). The block diagram representation of this model is shown in Figure 4.

The compressor model is composed by a static compressor map, used to determinate the air flow rate through the compressor, and by a dynamic model of the system inertia, which determines the compressor speed used to find the air flow rate. The state in the model is the compressor speed $\omega_{cp}$. The inputs to the model are the air pressure $p_{atm}$ and temperature $T_{atm}$ (atmospheric), the supply manifold pressure $p_{sm}$ (downstream pressure) and the voltage command of the compressor voltage $v_{cm}$.

The compressor flow map can be normally found in the device manufacturer data-sheet. In Pukrushpan et al. (2004) the Jensen & Kristensen map regression method is presented to compute the compressor air flow rate, avoiding the use of look-up tables (not suitable for simulations).

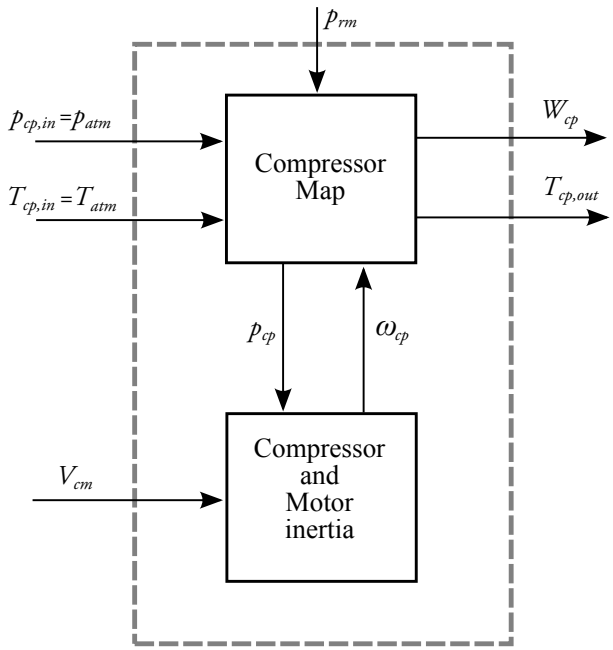


Fig. 4. Compressor model block diagram (Pukrushpan et al., 2004).

This method is presented with details in Pukrushpan et al. (2004) and the air flow rate $W_{cp}$ is computed using a regression algorithm on the compressor map and the compressor diameter $d_c$ in m, the air density $\rho_a$ in kg/m$^3$, and the air gas constant $\mathcal{R}_a$.

A look-up table is used to obtain the compressor efficiency $\eta_{cp}$. Then the temperature of the air leaving the compressor is then computed by:

$$T_{cp} = T_{atm} + \frac{T_{atm}}{\eta_{cp}} \left[ \left( \frac{p_{sm}}{p_{atm}} \right)^{\frac{\gamma-1}{\gamma}} - 1 \right] \tag{1}$$

Then the torque required to drive the compressor, is given by:

$$\tau_{cp} = \frac{C_p}{\omega_{cp}} \frac{T_{atm}}{\eta_{cp}} \left[ \left( \frac{p_{sm}}{p_{atm}} \right)^{\frac{\gamma-1}{\gamma}} - 1 \right] W_{cp} \tag{2}$$

where the torque $\tau_{cp}$ is in N.m and $C_p$ is the specific heat capacity of the air equals 1004 J.kg$^{-1}$.°K$^{-1}$. Both the temperature equation (1) and the torque equation (2) of the compressor are derived from turbine literature. The dynamic speed-inertia equation is given by:

$$J_{cp} \frac{d\omega_{cp}}{dt} = (\tau_{cm} - \tau_{cp}) \tag{3}$$

with $J_{cp}$ the combined compressor and motor inertia in kg.m$^2$, $\omega_{cp}$ the compressor speed in rad/sec, and $\tau_{cm}$ the compressor motor torque input.

Substituting equation (2) into equation (3) yields to the final expression for the supply manifold dynamic.

Today the use of permanent magnet DC motor is attractive due to efficiency and performance. In that case the voltage equation for the DC machine is:

$$v_{cm} = i_{cm} R_{cm} + v_{cm,ind} \tag{4}$$

The induced voltage and torque $\tau_{cm}$ are given by:

$$v_{cm,ind} = k_v \omega_{cp} \tag{5}$$
$$\tau_{cm} = k_t i_{cm} \tag{6}$$

The second compressor model presented in this section is a linear compressor model proposed in Gasser (2006). The diagram representation of this model is shown in Figure 5.

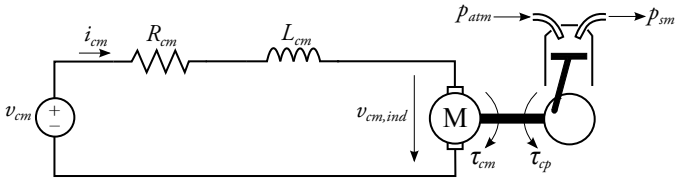


Fig. 5. Compressor model diagram (Gasser, 2006).

The voltage equation of the circuit is given by:

$$v_{cm} = L_{cm} \frac{di_{cm}}{dt} + R_{cm} i_{cm} + k_m \omega_{cp} \tag{7}$$

The torque equation of the system is given by equation (3) and the DC machine torque equation is given by equation (6), as the DC machine of the compressor-motor proposed in Gasser (2006) is also a permanent magnet DC motor.

The torque of the compressor is obtained by:

$$\tau_{cp} = k_p (p_{atm} - p_{sm}) \tag{8}$$

For the compressor characteristic, the relationship between the output mass flow rate $W_{cp}$ and the compressor speed $\omega_{cp}$ is assumed to be linear by a factor $k_{m,cp}$. A friction torque $\tau_{fric} = k_f \omega_{cp}$ is also considered in the equations. The complete linear model for the compressor-motor system is given by:

$$\begin{bmatrix} \frac{di_{cm}}{dt} \\ \frac{d\omega_{cp}}{dt} \\ \frac{dp_{sm}}{dt} \end{bmatrix} = \begin{bmatrix} -\frac{R_{cm}}{L_{cm}} & -\frac{k_e}{L_{cm}} & 0 \\ \frac{k_t}{J_{cp}} & -\frac{k_d}{J_{cp}} & -\frac{k_p}{J_{cp}} \\ 0 & \frac{\mathcal{R}T k_{m,cp}}{V_{sm}\mathcal{M}_{air}} & -\frac{\mathcal{R}T}{V_{sm}\mathcal{M}_{air}k_h} \end{bmatrix} \begin{bmatrix} i_{cm} \\ \omega_{cp} \\ p_{sm} \end{bmatrix} + \begin{bmatrix} \frac{1}{L_{cm}} & 0 \\ 0 & \frac{k_p}{J_{cp}} \\ 0 & \frac{\mathcal{R}T}{V_{sm}\mathcal{M}_{air}k_h} \end{bmatrix} \begin{bmatrix} v_{cm} \\ p_{atm} \end{bmatrix} \tag{9}$$

The system output is:

$$\begin{bmatrix} W_{cp} \\ p_{sm} \end{bmatrix} = \begin{bmatrix} 0 & k_{m,cp} & 0 \\ 0 & 0 & 1 \end{bmatrix} \begin{bmatrix} i_{cm} \\ \omega_{cp} \\ p_{sm} \end{bmatrix} \tag{10}$$

Using the test-bench set-up preseted before and the input signals presented in Figure 6, we obtain the parameter identification results for this second model. The identification results are resumed in Table 1. The linear model proposed by Gasser (2006) was found to be well adapted to the design of the compressor system control for mainly two reasons: identification results were good and this model includes the dynamic of the compressor motor current, which will be used later to consider a true autonomous system. The model response compared to measured data are compared in Figures 7 and 8.

Table 1. Identification results for the model proposed by (Gasser, 2006)

| Parameter | Identified Values | Units |
|---|---|---|
| $k_{m,cp}$ | $1.7002 \times 10^{-6}$ | $\frac{kg}{rad}$ |
| $k_h$ | $6088.1 \times 10^4$ | $Pa.s/kg$ |
| $k_p$ | $3.7477 \times 10^{-6}$ | $m^3$ |
| $k_e$ | 0.2634 | $V\frac{s}{rad}$ |
| $k_t$ | 0.1936 | $N.m/A$ |
| $k_d$ | 0.0588 | $N.m\frac{s}{rad}$ |
| $J_{cp}$ | $2.4637 \times 10^{-5}$ | $kg.m^2$ |
| $R_{cm}$ | 2.1805 | $\Omega$ |
| $L_{cm}$ | 0.0040 | $H$ |
| $V_{sm}$ | 0.0010 | $m^3$ |
| $k_p$ (PI) | 0.4912 | – |
| $k_i$ (PI) | 5.9854 | – |

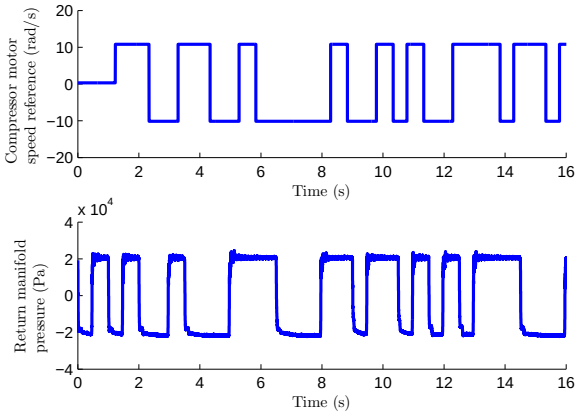


Fig. 6. Inputs for compressor model identification.

## 3. AIR SUPPLY CONTROL

In this section, a control strategy for the compressor system using the linear model and the robust control methods is proposed. The air input dynamic behaviour plays a very important role on the FC dynamic. The control objectives for the compressor system are chosen to comply with the desired performance of the FC. Two main objectives are considered: keep a desired oxygen excess ratio $\lambda_{O_2}$ and maximizing the net power delivered to the load. Note that we consider an autonomous system, i.e., the compressor energy is taken from the DC bus. This is not an easy requirement to meet, a trade-off has to be made because

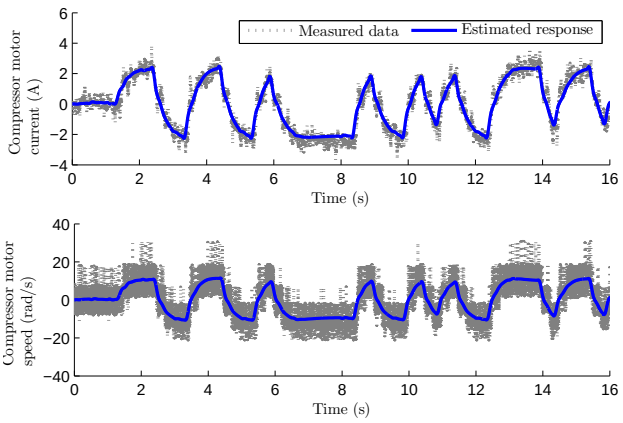


Fig. 7. Identification results of compressor model proposed by Gasser (2006).

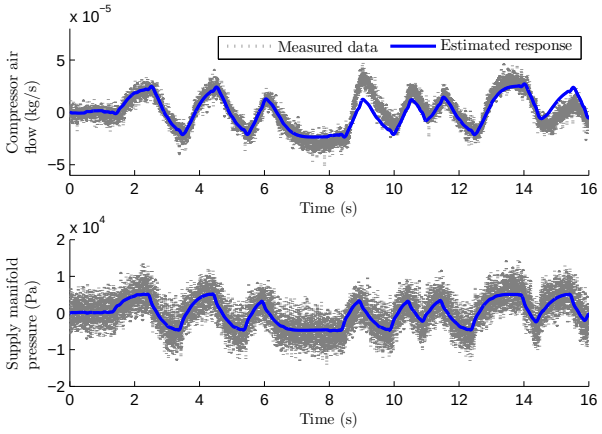


Fig. 8. Identification results of compressor model proposed by Gasser (2006).

rising the supply manifold pressure increases the FC performance, but rising the pressure increases the current consumed by the compressor directly from the FC stack itself. In a simplistic solution, this is partially achieved minimizing the overshoots and properly rejecting disturbance transients on the supply manifold pressure and on the compressor speed. Note that at higher speeds more current is consumed by the compressor-motor. The compressor system dynamic is composed by the compressor-motor and the FC supply manifold dynamic. The control strategies described in this section are motivated by the test-bench and the air compressor for operation of the FC under dry air conditions.

Note that considering an autonomous system the following system currents relationship can be established:

$$I_{DC} = I_{load} + I_{cm} \tag{11}$$

were $I_{DC}$ is the current delivered by the hybrid boost converters at the DC bus.

We will present now the classic strategy used to obtain a simple PI controller for this system.

### 3.1 Classic control approach

A very simple control design for a PI is presented. We used the function `sisotool` in MATLAB to find a PI controller that satisfies a gain margin larger than 6dB and a phase margin larger than 45°. A design that presents a good trade-off between the overshoot and a stabilization time $t_s$ around 2s was chosen. The controller found satisfies $GM = 12.2$dB and a $PM = 60°$. The gains are given by $k_p = 8.33 \times 10^4$ and $k_i = 5.21 \times 10^5$. This PI controller for $K_{\lambda_{O_2}}$ has the classic structure $K_{\lambda_{O_2}} = k_p + k_i/s$.

A proposed strategy for oxygen excess ratio control is presented in Figure 9. In this case the speed controller $K_\omega(s)$ is given by the identified PI controller with gains $k_p = 0.4912$ and $k_i = 5.9854$.

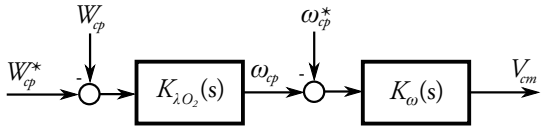


Fig. 9. Compressor proposed control strategy.

Time-domain simulations results are computed for the closed-loop system and step inputs are applied to the FC current $I_{fc}$ simulating changes in the load current. The simulation result is presented in Figure 10 for ±20% load steps. Figure 11 show the compressor flow error ($W^*_{cp} - W_{cp}$) to obtain the desired oxygen excess ratio. Results are compared to the open-loop system (no control). The system regulation to the desired $\lambda_{O_2} = 1.6$ is effectively achieved. In Pukrushpan et al. (2004) this value was fixed at 2 and was chosen for the maximum net power delivered to the load. In our case, after several tests on the real FC stack, this value was fixed to 1.6, for which the best performance was obtained for the FC operating under dry air conditions (without humidification) in terms of the FC stack voltage stabilization.

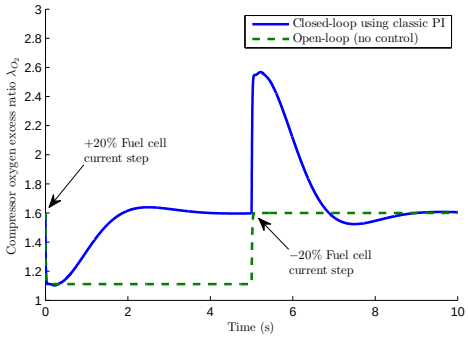


Fig. 10. Oxygen excess ratio using linear model.

### 3.2 Robust control approach

In the robust control approach we compute both full and reduced order $\mathcal{H}_\infty$ controllers. The compressor system block diagram is presented in Figure 13 for the system proposed by Gasser (2006). The proposed control configuration with a single performance weighting function is presented in Figure 12.

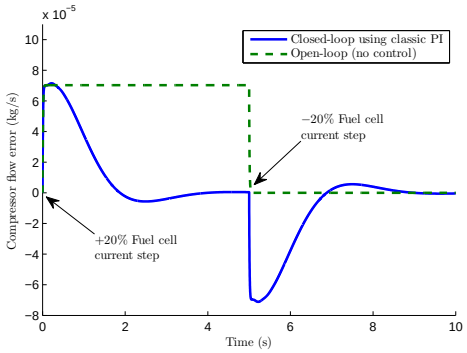


Fig. 11. Oxygen excess ratio using linear model.

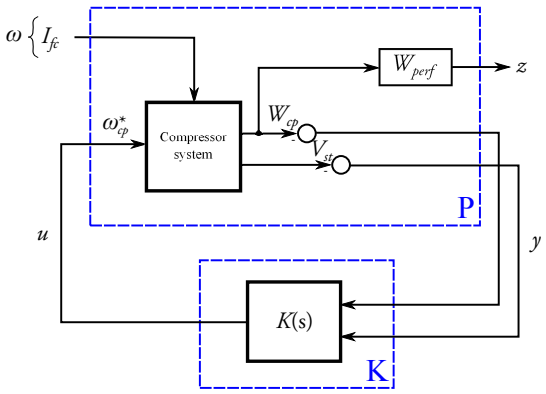


Fig. 12. Control configuration in the P-K form for the compressor system.

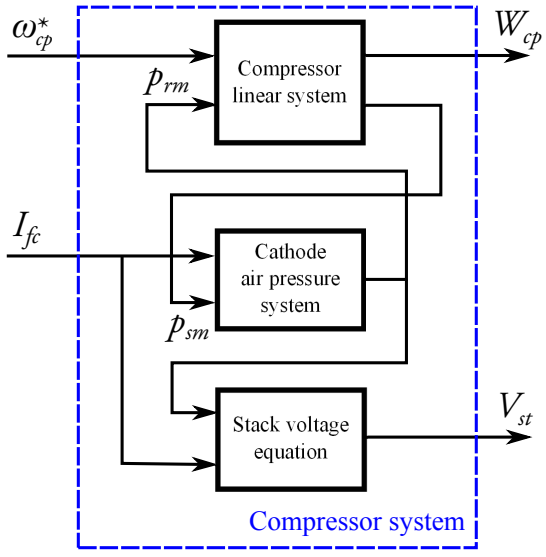


Fig. 13. Compressor system block diagram.

The weighting function is fixed for a stabilization time $t_s = 1$s. Using the classic 5% criterion and the approximation to dominant poles, the expression $t_s = \frac{3}{\zeta\omega_n}$ can be used to obtain the natural frequency of the desired closed-loop. With $\zeta = 0.6$, we obtain $\omega_n = 5$rad/s. The performance weight is then given by:

$$W_{perf} = \frac{0.5s + 5}{s + 5 \times 10^{-8}} \tag{12}$$

The full order $\mathcal{H}_\infty$ controller (order 5) obtained can be reduced to $1^{st}$ order system, given by:

$$K_{\mathcal{H}_\infty}(s) = \begin{bmatrix} \dfrac{2.587 \times 10^5 s + 7.036 \times 10^5}{s - 0.0001521} \\ \dfrac{9.747 \times 10^{-5} s + 2.543 \times 10^{-8}}{s - 0.0001521} \end{bmatrix}$$

A robust controller was also computed using the function `hinfstruct` and fixing the controller structure to a MIMO PI. The closed-loop $\mathcal{H}_\infty$ gain for each robust controller found are summarized in Table 2. The singular values plots of the sensitivity functions are compared in Figure 14. A slightly more robust controller is obtained with the full and reduced order $\mathcal{H}_\infty$ controllers.

Table 2. Closed-loop $\mathcal{H}_\infty$ gain

| Controller | Performance |
|---|---|
| Full order $\mathcal{H}_\infty$ | $\mathcal{H}_\infty < 0.0788$ |
| Reduced order $\mathcal{H}_\infty$ | $\mathcal{H}_\infty < 0.1848$ |
| Using `hinfstruct` | $\mathcal{H}_\infty < 0.1865$ |
| Classic PI | $\mathcal{H}_\infty < 0.1933$ |

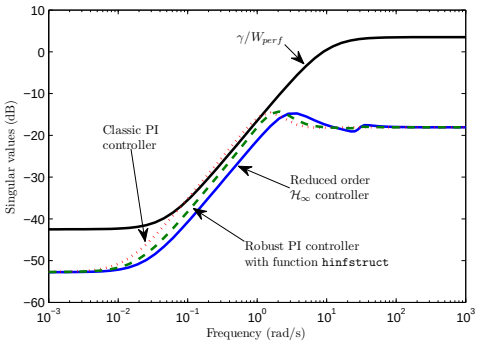


Fig. 14. Closed-loop singular values plot.

In Figures 15 and 16 the controllers regulation of the oxygen excess ratio are compared using the linear and non-linear models (cf to models equations (9) and (**??**) in chapter **??**). The reduced order $\mathcal{H}_\infty$ controller is not shown in the non-linear simulations because the results obtained are very similar to those obtained with the full order $\mathcal{H}_\infty$ control. In the linear simulation 20% load step are applied. In the non-linear case a 75% load step is applied. The non-linear simulation results show a clearly better disturbance rejection using the proposed robust control. The Figure 17 show the evolution of the net power delivered by the FC after a series of load steps. Note the several overshoots in the transient response using the classic control. Using the same series of load step a different set of system variables is presented in Figure 18.

Using the non-linear model of the compressor system, validation of robust controller is obtained. Dynamic variations on the operating point of the FC polarization curve and the compressor flow map are presented in Figures 19 and 20 respectively after ±75% load steps. According with these results, and associating these results with the overshoot peaks shown in Figures 16 and 17, an improvement of the net power delivered by the FC is obtained with the MIMO $\mathcal{H}_\infty$ control methodology. The evolution of the operating point in the polarization curves given an idea of the degradation of cell performance after a big load current step, and the influence of the supply manifold pressure $p_{sm}$ variation.

Finally, several other dynamic results are obtained using the non-linear model, and applying a second series of load steps. A final result sequence is given in Figure 21. Note the slight oscillatory behavior of the compressor motor speed using the classic methodology. A smooth disturbance rejection is achieved on the supply manifold pressure. When comparing with results presented in Figure 18, these results obtained with the linear and non-linear models are very similar. Figure 21 shows the good regulation of the compressor speed and the drop on the FC stack voltage after the disturbances.

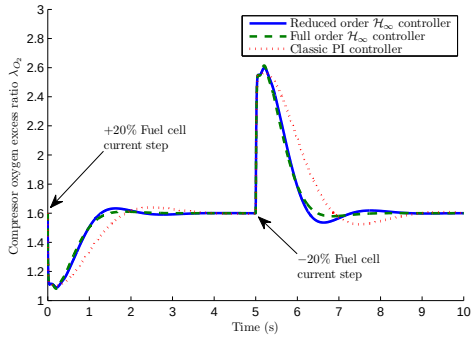


Fig. 15. Oxygen excess ratio simulation results using linear model.

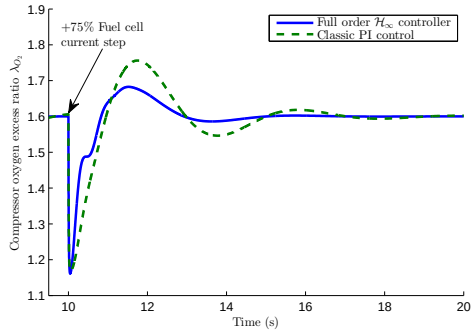


Fig. 16. Oxygen excess ratio simulation results using non-linear model.

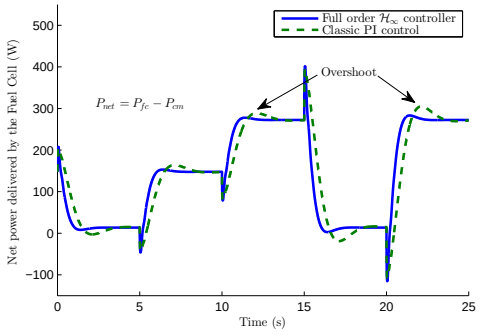


Fig. 17. Net power delivered by the FC.

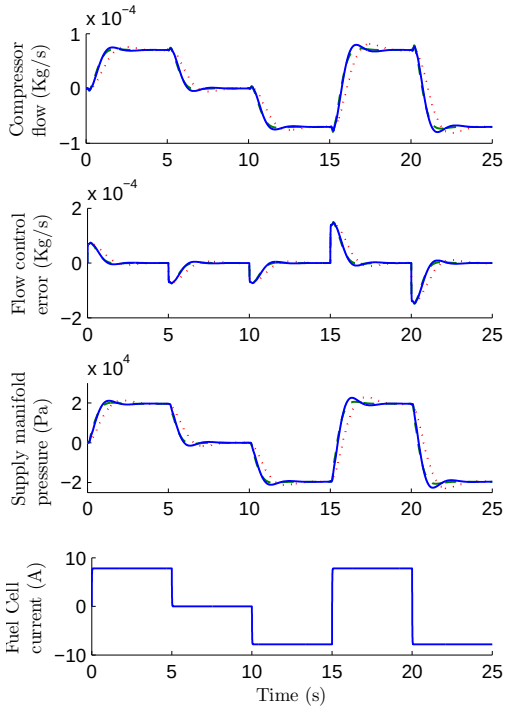


Fig. 18. Simulation results using linear model (reduced order controller in continuous line, full order controller in dashed line and classic PI controller in dotted line).

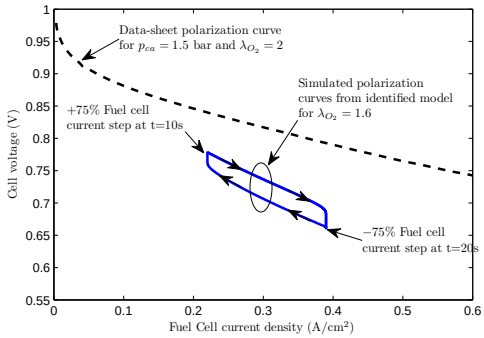


Fig. 19. Polarization curve.

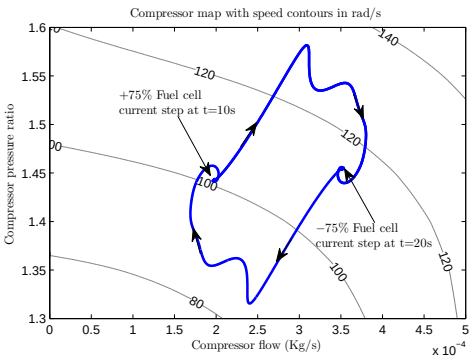


Fig. 20. Compressor map.

## 4. CONCLUSION

A reduced order robust control with $\mathcal{H}_\infty$ performance is presented in this paper. The results obtained were satifatory when compared to a classical controller using PI control in terms of robustness and dynamics. The proposed control is multivariable with the advantage of implementation on a real system by using a reduced order controller. The obtained controller performance was validated using the non-linear model of the FC air supply system. A near future perspective in this work is the control validation on the real-time test-bench set-up.

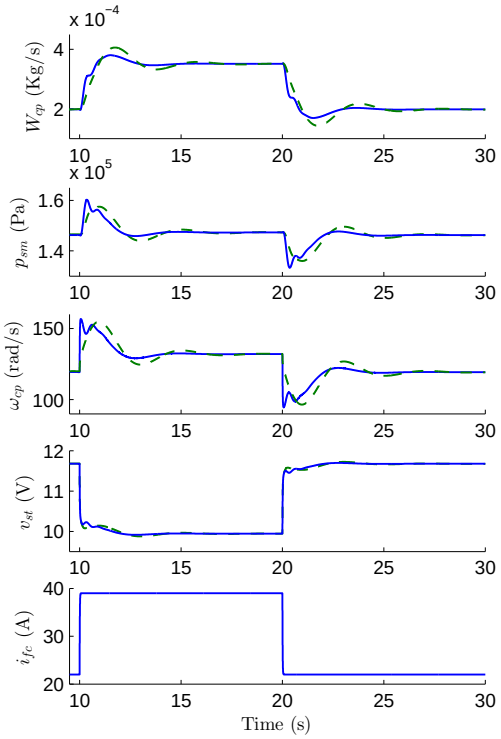


Fig. 21. Simulation results using non-linear model (reduced order controller in continuous line and classic PI control in dotted line).

## REFERENCES


Chang, Y.A. and Moura, S.J. (2009). Air Flow Control in Fuel Cell Systems: An Extremum Seeking Approach . In *American Control Conference, ACC 2009*, 4299–4304.

Gasser, F. (2006). *An Analytical, Control-Oriented State Space Model for a PEM Fuel Cell System*. Ph.D. thesis, École Polytechnique Fédérale de Laussane.

Grujicic, M., Chittajallu, K.M., Law, E.H., and Pukrushpan, J.T. (2004). Model-based control strategies in the dynamic interaction of air supply and fuel cell. *Proc. Instn Mech. Engrs., Part A: J. Power and Energy*, 218.

Hernandez-Torres, D., Riu, D., and Sename, O. (2012). An LPV Control Approach for a Fuel Cell Power Generator Air Supply System. In *American Control Conference, ACC 2012*, 4299–4304.

Hernandez-Torres, D., Riu, D., Sename, O., and Druart, F. (2011). A robust multivariable approach for hybrid fuel cell supercapacitor power generation system. *European Physical Journal of Applied Physics*, 54(2).

Na, W.K. and Gou, B. (2008). Feedback-Linearization-Based Nonlinear Control for PEM Fuel Cells. *IEEE Transactions on Energy Conversion*, 23(1), 179–190.

Pukrushpan, J.T., Stefanopoulou, A.G., and Peng, H. (2004). *Control of Fuel Cell Power Systems. Principles, Modeling, Analysis and Feedback Design.* Springer.

Talj, R., Ortega, R., and Hilairet, M. (2009). A controller tuning methodology for the air supply system of a PEM fuel-cell system with guaranteed stability properties. *International Journal of Control*, 82(9), 1706–1719.

Tekin, M., Hissel, D., Pera, M., and Kauffmann, J. (2006). Energy consumption reduction of a PEM fuel cell motor-compressor group thanks to efficient control laws. *Journal of Power Sources*, 156, 57–63.

Wang, F., Chen, H., Yang, Y., and Yen, J. (2008). Multivariable robust control of a proton exchange membrane fuel cell system. *Journal of Power Sources*, 177, 393–403.

Wang, F. and Ko, C. (2010). Multivariable robust PID control for a PEMFC system. *International Journal of Hydrogen Energy*, 35, 10437–10445.